



OPEN

Significance of Hall effect and Ion slip in a three-dimensional bioconvective Tangent hyperbolic nanofluid flow subject to Arrhenius activation energy

Muhammad Ramzan^{1,2}, Hina Gul¹, Jae Dong Chung², Seifedine Kadry³ & Yu-Ming Chu^{4,5}✉

The dynamics of partially ionized fluid flow subjected to the magnetic field are altogether distinct in comparison to the flow of natural fluids. Fewer studies are available in the literature discussing the alluring characteristics of the Hall effect and the Ion slip in nanofluid flows. Nevertheless, the flow of nanofluid flow with Hall and Ion slip effect integrated with activation energy, gyrotactic microorganisms, and Cattaneo–Christov heat flux is still scarce. To fill in this gap, our aim here is to examine the three dimensional electrically conducting Tangent hyperbolic bioconvective nanofluid flow with Hall and Ion slip under the influence of magnetic field and heat transmission phenomenon past a stretching sheet. Impacts of Cattaneo–Christov heat flux, Arrhenius activation energy, and chemical reaction are also considered here. For the conversion of a non-linear system to an ordinary one, pertinent transformations procedure is implemented. By using the `bvp4c` MATLAB function, these equations with the boundary conditions are worked out numerically. The significant impacts of prominent parameters on velocity, temperature, and concentration profiles are investigated through graphical illustrations. The results show that the velocity of the fluid is enhanced once the Ion slip and Hall parameters values are improved. Furthermore, the concentration is improved when the values of the activation energy parameter are enhanced.

List of symbols

a, b	Dimensional constant
Pr	Prandtl number
λ^*	Porosity parameter
Γ	Transient material constant
k	Thermal conductivity of nanofluid
β_i	Ion slip parameter
Q	Heat generation parameter
τ_w	Drag force coefficient
Bi	Biot number
T	Liquid temperature
μ	Dynamic viscosity of the liquid
λ_2	Thermal relaxation time
Ec	Eckert number
E	Activation energy parameter
C_w	Wall concentration
B_0	Strength of magnetic field

¹Department of Computer Science, Bahria University, Islamabad 44000, Pakistan. ²Department of Mechanical Engineering, Sejong University, Seoul 143-747, South Korea. ³Department of Mathematics and Computer Science, Faculty of Science, Beirut Arab University, Beirut 115020, Lebanon. ⁴Department of Mathematics, Huzhou University, Huzhou 313000, People's Republic of China. ⁵Hunan Provincial Key Laboratory of Mathematical Modeling and Analysis in Engineering, Changsha University of Science and Technology, Changsha 410114, People's Republic of China. ✉email: chuyuming@zjhu.edu.cn

V_w	Stretching velocity
N_b	Parameter of Brownian motion
D_B	Coefficient of Brownian diffusion
τ	Surface shear stress
Sc	Schmidt number
T	Liquid temperature
M	Magnetic parameter
Lb	Bio convection Lewis number
Sh_x	Sherwood number
n	Density motile of microorganisms
B	Slip parameter
N_∞	Ambient concentration of microorganisms
K_r	Chemical reaction parameter
γ	Thermal relaxation parameter
Ω	Microorganisms concentration difference parameter
N_0	Reference concentration of microorganisms
(u, v, w)	Components of velocities
C_{fx}, C_{gy}	Drag force
F_r	Inertia coefficient
σ	Stefan–Boltzmann constant
δ	Fluid parameter
β_e	Hall parameter
Re_x	Reynolds number
T_w	Temperature on wall
We	Weissenberg number
ρ	Density of fluid
ν	Kinematic viscosity
q_m	Mass flux
C	Liquid concentration
C_f	Drag force
c_p	Capacity of specific heat
C_∞	Fluid concentration
λ	Stretching ratio parameter
N_t	Parameter of thermophoresis
Nn_x	Local density number
Re_x	Reynolds number
D_T	Coefficient of thermophoretic diffusion
T_∞	Diffusive temperature
K_c	Coefficient of chemical reaction
Pe	Bio-convection Peclet number
D_m	Microorganism diffusion coefficient
W_c	Maximum cell swimming speed
q_n	Wall motile organism flux
D_n	Diffusivity of microorganism
h_f	Heat transfer coefficient
E_a	Coefficient of activation energy
Q_0	Coefficient of heat absorption
T_w	Temperature on wall

The investigation of non-Newtonian liquids is of prime value owing to their industrial and engineering applications. A single constitutive relation can't be quoted to exhibit the characteristics of such fluids. China clay, soup, toothpaste, shaving creams, blood at a small shear rate, and mayonnaise, etc. are examples of non-Newtonian liquids. Owing to their interesting applications, researchers have described different models of non-Newtonian liquids. Amongst these, the Tangent hyperbolic liquid model is of vital importance that can forecast the shear-thinning phenomenon with marvelous accuracy. The usage of this model in industry and laboratory experiments is recommended by researchers and scientists. Melts, whipped cream, ketchup, and blood are some examples of Tangent hyperbolic fluid. Tangent hyperbolic fluid is a kind of non-Newtonian fluid model which falls in the category of rate type fluids and whose equations are true for both strong and weak shear stresses. In the case of shear-thinning, the rate will dominate the shear stress and vice versa in the case of shear thickening. In 1929, Williamson anticipated a model named “Williamson fluid” with pseudoplastic materials features of shear-thinning and substantiated its results experimentally. Examples of this fluid may include polymer solutions/melts, nail polish, blood, etc. However, the Tangent hyperbolic fluid model has an edge over its contemporary models owing to its unique features of computational comfort, simplicity, and physical robustness. Shafiq et al.¹ found an analytical solution of Tangent hyperbolic bio-convective nanomaterial flow holding motile microorganisms by using the Homotopy Analysis Method (HAM). They perceived that for strong magnetic effects, the velocity profile reduces. They also witnessed an opposite behavior of concentration and temperature profiles for mounting estimates of the thermophoresis parameter. Hayat et al.² explored MHD Tangent hyperbolic nanomaterial flow with variable thickness. From this study, it is comprehended that velocity is a decreased for growing estimations

of the Weissenberg number and magnetic parameter. Ibrahim and Gizewu³, addressed the Tangent hyperbolic nanofluid flow with double diffusion effects and a second-order slip condition at the boundary. Ramzan et al.⁴ discussed the second-order slip in the attendance of Cattaneo–Christov (C–C) heat flux and homogeneous–heterogeneous reactions with Tangent hyperbolic liquid flow. The flow behavior of Tangent hyperbolic liquid (blood) with copper nanoparticles over a ciliated tube is studied by Maqbool et al.⁵. Some more recent investigations highlighting various aspects of Tangent hyperbolic fluid flow may be seen at Refs.^{6–9} and many therein.

Arrhenius activation energy is the least essential energy mandatory to initiate a chemical reaction. It is coined by Arrhenius in 1889. Activation energy plays the role of an obstacle between un-reacted and reacted molecules or atoms. Once this barrier is crossed, the chemical reaction will occur, and, in such situations, only those molecules or atoms will cross the barricade that has more energy than the fence. Awad et al.¹⁰ analyzed the impacts of activation energy and binary chemical reaction in a viscous rotating flow utilizing the Spectral relaxation method (SRM). It is revealed that concentration distribution is increased once the values of dimensionless activation energy are boosted. It is also noticed that the velocity field is monotonically decayed versus a feeble fluid rotation rate. Lu et al.¹¹ studied numerically a 3D nano liquid flow past a moving elongated plate with combined impacts of Arrhenius activation energy and binary chemical reaction. The proposed mathematical model is also accompanied by gyrotactic microorganisms, Joule heating, thermal radiation with anisotropic slip at the boundary. It is disclosed that microorganism's local density declines versus nondimensional activation energy. The flow of second-grade nano liquid flow with the Arrhenius activation energy and binary chemical reaction in a spongy media is studied numerically by Khan et al.¹². The flow analysis also caters to the behaviors of thermal radiation and Entropy generation. It is stated that the concentration is declined for large values of chemical reaction and activation parameters. Koriko et al.¹³ studied the flow of Micropolar fluid with Exothermic and Endothermic chemical reactions past a vertical permeable stretched surface. Some recent attempts discussing activation energy may be found at Refs.^{11,14–16}.

The convective movement of fluid at the microscopic level owing to the density gradient is termed as Bio-convection and is generated by the swimming of motile organisms. The density of the customary fluid is enhanced by self-driven microorganisms in a specific direction thus generating bio-convection. A good number of applications in wastewater, agriculture, soil, and microbial engineering may be found in the real world associated with bioconvective microorganisms. The idea of bioconvective nanofluid was coined by Kuznetsov^{17,18}. Kuznetsov¹⁹ focused to visualize the effect of nano-liquid with gyrotactic microorganisms. Aziz et al.²⁰ examined the steady boundary layer flow in a porous medium with an amalgamation of gyrotactic microorganisms and nano-liquid. The behavior of bioconvective magnetic field, thermophoresis, and Brownian motion on a free convection nano-liquid flow comprising the gyrotactic microorganisms over an elongating sheet is explored by Akbar and Khan²¹. Alsaedi et al.²² introduced the effect of nanofluid with gyrotactic microorganisms. Lately, Khan et al.²³ deliberated the effect of generalized Burgers liquid flow with chemical reactions and magneto nanoparticle. The variable thermophysical effects on bioconvective nano-liquid are examined by Begum et al.²⁴. More studies highlighting the role of bio-convection are appended at Refs.^{11,25–29}.

In all the above-quoted works, the impacts of Hall and Ion slip are not considered in employing the ohm's law as there is no significant effect for the tenuous magnetic field. Nevertheless, nowadays applications of magnetohydrodynamics are preferred with the strong applied magnetic field so that the impact of magnetohydrodynamics is perceptible. That is why the Hall and Ion slip are vital and they have significant effects on the magnitude, the current density's direction, and subsequently on the magnetic force term³⁰. The behavior of ionized fluids under the effect of the magnetic field has entirely different traits in comparison to the non-ionized fluids. The ionized fluids are influenced by three major factors named (i) the magnetic force owing to an applied magnetic field, (ii) the Hall force, because of electrons' collision, (iii) the Ion slip force, owing to ions' collision. Most of the existing works state the flows influenced by the Lorentz force. Fewer studies may be found with Hall's current effects. But the literature highlighting the impacts of both Ion and hall slip is scarce. Abdelsalam and Bhatti³¹ studied the Tangent hyperbolic nanofluid peristaltic flow influenced by chemical reaction and Ion and Hall slip impacts in a non-uniform channel. The prime outcome of the study is that the chemical reaction depicts dual solutions for the concentration profile for higher estimates of the Brownian motion parameter. The flow of nanofluid comprising varied metallic particles and their oxides like copper, silver, and aluminum oxide are immersed into the blood with Ion and Hall slip effects amalgamated with heat generation/absorption is deliberated by Nawaz et al.³². It is revealed that the application of Ion and Hall slip results in a substantial decrease in heat dissipation in the presence applied magnetic field. A comparative analysis of two types of nanofluid flows namely 36 nm Al_2O_3 -water and 47 nm Al_2O_3 -water over an upper horizontal surface of a paraboloid is analyzed in the attendance of Hall effect by Animasaun et al.³³. It is observed in this study that cross fluid velocity in the case of 36 nm nanoparticles is dominant in comparison to the 47 nm nanoparticles. Recent studies focusing on Hall and Ion slip effect may be found at Refs.^{34,35}.

In the present era, the alluring characteristics of the nanofluids have attracted researchers and scientists to dig out new avenues. The nanofluid is an engineered fluid comprising an amalgamation of metallic particles or their associated oxides and some customary liquid like water. The heat transfer capabilities of nanofluids are amazingly much higher than those of the routine liquids. This tempting feature of nanofluids is so captivating that it has revolutionized the modern technological world. One can find its applications from the cooling of microchips to atomic reactors. The latest studies emphasizing various attributes of nanofluids may be found in Refs.^{36–43}. Additionally, copious applications under the impact of the magnetic field may be found in engineering, medicine, and physics. Fluids under magnetic field influence have interesting applications like MHD generators, treatment of tumors, and pumps, etc. The strength of the applied magnetic field and arrangements of molecules highly affects the fluids' behavior. The application of the magnetic field alters the arrangement of nanoparticles and eventually the concentration of the fluid. A nanofluid with magnetic physiognomies is termed as magnetic

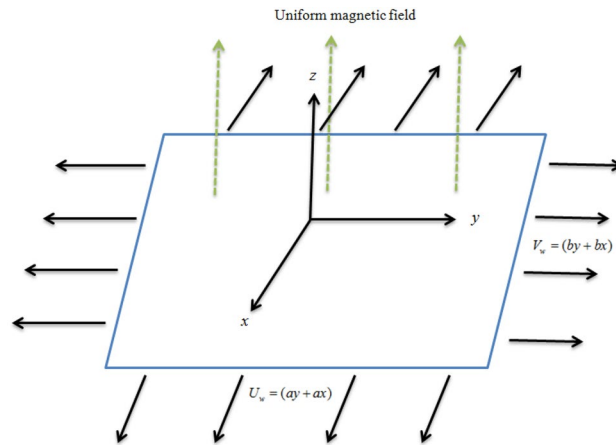


Figure 1. Flow geometry.

nanofluid with vast range applications including optical modulators and switches. A good number of magneto-nanofluids explorations may be found in the literature^{44–46}.

The aforesaid literature review reveals that very few explorations are discussed that signifies the partially ionized nanofluid flows. However, no study so far carried out that communicates the activation energy amalgamated in a partially ionized Tangent hyperbolic nanofluid flow under the influence of magnetohydrodynamics. The additional attributes of Cattaneo–Christov heat flux with convective boundary condition in the envisioned mathematical model also distinguish the present study from the existing literature. The consideration of these impacts turns the problem into a highly nonlinear system. The numerical solution of the problem is uncovered by using the Runge–Kutta-4 technique with the shooting method. The manuscript is structured in five sections. The modeling of the envisioned problem is given in “[Mathematical formulation](#)”. The numerical solution method is presented in “[Numerical computations](#)”. “[Results and discussion](#)” is devoted to graphical and numerical results’ discussion. The concluding comments emphasizing key results are presented in the last section.

While studying this exploration, we will try to answer the subsequent questions:

- i. What is the effect of Hall and Ion slip on the fluid velocity?
- ii. What is the role of activation energy in this model?
- iii. How “bioconvection” affect the motile density profile?
- iv. Does the temperature of the fluid is influenced by the magnetic field effect?
- v. How Cattaneo–Christov heat flux contributes to the nanofluid flow?

Mathematical formulation

Let us assume heat transfer in partially ionized 3D tangent hyperbolic nano liquid past a surface with velocity $V_w = [(x + y)a, (y + x)b]$, Conversion of activation energy, Chemical reaction, bioconvective gyrotactic organisms with CC heat flux and Ohmic dissipation likewise consider (Fig. 1).

The boundary layer governing equations depicting the assumed model is^{11,31,47}:

$$u_x + v_y + w_z = 0, \tag{1}$$

$$uu_x + vv_y + ww_z = (1-n)vu_{zz} + n\sqrt{2}\nu\Gamma u_z u_{zz} + \frac{\sigma B_0^2}{\rho[\beta_e^2 + (1 + \beta_e\beta_i)^2]} [\beta_e v - (1 + \beta_e\beta_i)u] - \frac{\nu}{K} u - Fu^2, \tag{2}$$

$$uv_x + vv_y + ww_z = (1-n)vv_{zz} + n\sqrt{2}\nu\Gamma v_z v_{zz} - \frac{\sigma B_0^2}{\rho[\beta_e^2 + (1 + \beta_e\beta_i)^2]} [\beta_e u - (1 + \beta_e\beta_i)v] - \frac{\nu}{K} v - Fv^2, \tag{3}$$

$$u \frac{\partial T}{\partial x} + v \frac{\partial T}{\partial y} + w \frac{\partial T}{\partial z} = \frac{k}{\rho c_p} \frac{\partial T}{\partial z} - \lambda_2 \left(\begin{aligned} &u^2 \frac{\partial^2 T}{\partial x^2} + v^2 \frac{\partial^2 T}{\partial y^2} + w^2 \frac{\partial^2 T}{\partial z^2} + (uu_x + vv_y + ww_z) \frac{\partial T}{\partial x} \\ &+ (uv_x + vv_y + ww_z) \frac{\partial T}{\partial y} \\ &+ (uw_x + vw_y + ww_z) \frac{\partial T}{\partial z} + 2uv \frac{\partial^2 T}{\partial xy} + 2vw \frac{\partial^2 T}{\partial yz} + 2uw \frac{\partial^2 T}{\partial xz} \end{aligned} \right) \tag{4}$$

$$+ \frac{Q_0}{\rho c_p} \left(T - T_\infty \right) + \tau D_B C_z \frac{\partial T}{\partial z} + \tau \frac{DT}{T_\infty} \frac{\partial T}{\partial z} + \frac{\sigma B_0^2}{\rho[\beta_e^2 + (1 + \beta_e\beta_i)^2]} [u^2 + v^2],$$

$$u C_x + v C_y + w C_z = D_B C_{zz} + \frac{D_T}{T_\infty} \frac{T^*}{T_\infty} - K_c^2 (C - C_\infty) \left(\frac{T^*}{T_\infty} \right)^n e^{-\frac{E_a}{k T^*}}, \tag{5}$$

$$u N_x + v N_y + w N_z + \frac{b W_c}{(C_w - C_\infty)} [N_z C_z + N C_{zz}] = D_n N_{zz}, \tag{6}$$

with associated suitable boundary conditions:

$$u = U_w = (y + x)a, \quad v = V_w = (y + x)b, \quad w = 0, \quad -k \frac{T^*}{z} = h_f (T_w^* - T^*), \quad C = C_w + \alpha C_z, \quad N = N_w, \quad \text{at } z = 0$$

$$u \rightarrow 0, \quad v \rightarrow 0, \quad T^* = T_\infty^*, \quad C = C_\infty, \quad N = N_\infty, \quad \text{as } z \rightarrow \infty. \tag{7}$$

Similarity transformations are defined as:

$$u = (x + y) a f', \quad v = (x + y) a g', \quad w = -(g + f) \sqrt{a v},$$

$$\theta = \frac{T^* - T_\infty^*}{T_w^* - T_\infty^*}, \quad \varphi = \frac{C - C_\infty}{C_w - C_\infty}, \quad \eta = \sqrt{\frac{a}{v}} z, \quad \xi = \frac{N - N_\infty}{N_w - N_\infty}. \tag{8}$$

Using Eq. (8), Eqs. (2)–(7) become:

$$(1 - n) f'''' + n W e f'' f'''' - \lambda * f' - F_r f'^2 + (g + f) f'' - f'^2 - g' f' + \frac{M^2}{\beta_e^2 + (1 + \beta_e \beta_i)^2} [g' \beta_e - f' (1 + \beta_i \beta_e)] = 0, \tag{9}$$

$$(1 - n) g'''' + n W e g'' g'''' + (f + g) g'' - g'^2 - g' f' - \lambda * g' - F_r g'^2 - \frac{M^2}{\beta_e^2 + (1 + \beta_e \beta_i)^2} [f' \beta_e + g' (1 + \beta_e \beta_i)] = 0, \tag{10}$$

$$\frac{1}{Pr} \theta'' - \gamma [(g + f)(f' + g')\theta' + (g + f)^2 \theta''] + Q\theta + N_b \theta' \varphi' + N_t \theta'^2 + \frac{M^2 Ec}{\beta_e^2 + (1 + \beta_e \beta_i)^2} (g'^2 + f'^2) + (g + f)\theta' = 0, \tag{11}$$

$$\varphi'' + Sc(g + f)\varphi' + \frac{N_t}{N_b} \theta'' - K_r Sc \varphi (1 + \delta \theta)^n e^{\frac{-E}{(1 + \delta \theta)}} = 0. \tag{12}$$

$$\xi'' + Lb(g + f)\xi' - Pe[(\Omega + \xi)\varphi'' + \xi'\varphi'] = 0, \tag{13}$$

with associated boundary conditions

$$f(0) = 0, \quad f'(0) = 1, \quad g(0) = 0, \quad g'(0) = \lambda, \quad \theta' = -Bi(1 - \theta), \quad \varphi(0) = 1 + B\varphi'(0), \quad \xi(0) = 1, \tag{14}$$

$$f'(\infty) = 0, \quad g'(\infty) = 0, \quad \theta(\infty) = 0, \quad \varphi(\infty) = 0, \quad \xi(\infty) = 0.$$

The above quantities are defined as

$$\beta_e = \omega_e \tau_e, \quad M^2 = \frac{\sigma B_0^2}{\rho a}, \quad \beta_i = \omega_i \tau_i, \quad Pr = \frac{\mu c_p}{k}, \quad Ec = \frac{U_w^2}{c_p (T_w - T_\infty)}, \quad \lambda = \frac{b}{a},$$

$$\gamma = \lambda_2 a, \quad Q = \frac{Q_0}{\rho c_p a}, \quad \delta = \frac{\Delta T}{T_\infty}, \quad N_b = \frac{\tau D_B C_\infty}{v}, \quad N_t = \frac{\tau D_T \Delta T}{T_\infty v}, \quad E = \frac{Ea}{k T_\infty}, \tag{15}$$

$$K_r = \frac{K_c^2}{a}, \quad Bi = \frac{h_f}{k} \sqrt{\frac{v}{a}}, \quad We = \frac{\sqrt{2a} \Gamma U_w}{\sqrt{v}}, \quad Lb = \frac{v}{D_m}, \quad \Omega = \frac{n_\infty}{n_f - n_\infty},$$

$$\beta_e = \omega_e \tau_e, \quad M^2 = \frac{\sigma B_0^2}{\rho a}, \quad \beta_i = \omega_i \tau_i, \quad Pe = \frac{b W_c}{D_m}.$$

Drag force coefficient in C_{fx} and C_{gy} , local Sherwood number and local density of the number of the motile microorganisms are defined by:

$$C_{fX} = \frac{\tau_{zX}|_{z=0}}{\rho a^2(x+y)^2}, \quad C_{gY} = \frac{\tau_{zY}|_{z=0}}{\rho a^2(x+y)^2}, \quad Sh_X = \frac{(x+y)q_m}{D_B(C_w - C_\infty)} \Big|_{z=0}, \quad Nn_X = \frac{(x+y)q_n}{D_n(n_f - n_\infty)}, \quad (16)$$

where

$$\tau_{zX} = [(1-n)u_z + \frac{n\Gamma}{\sqrt{2}}u_z^2]_{z=0}, \quad \tau_{zY} = [(1-n)v_z + \frac{n\Gamma}{\sqrt{2}}v_z^2]_{z=0}, \quad (17)$$

$$q_m = -D_B C_z|_{z=0}, \quad q_n = -D_n n_z|_{z=0}.$$

The dimensionless Skin friction coefficients, local Sherwood number, and local density number of the motile microorganisms are appended as follows:

$$C_{fX} \sqrt{Re_X} = (1-n)f''(0) + \frac{n}{2} We(f''(0))^2,$$

$$C_{gY} \sqrt{Re_X} = (1-n)g''(0) + \frac{n}{2} We(g''(0))^2, \quad (18)$$

$$Sh_X Re^{-0.5} = -\phi'(0), \quad Nn_X Re_X^{-1/2} = -\xi'(0).$$

With local Reynolds number

$$Re = \frac{U_w^2}{av}. \quad (19)$$

Numerical computations

The system of equations defined above is handled by the MATLAB software `bvp4c` tool. The infinite domain is taken as $\eta = 4$ which is sufficient to examine the asymptotic execution of the solution. The initial approximation with a tolerance 10^{-6} is acceptable to define a numerical solution. The initial conditions equivalent to the boundary conditions must meet the solution system. In this direction, First of all, new variables are introduced as:

$$f = Y_1, f' = Y_2, f'' = Y_3, f''' = Y_3', g = Y_4, g' = Y_5, g'' = Y_6,$$

$$g''' = Y_6', \theta = Y_7, \theta' = Y_8, \theta'' = Y_8', \varphi = Y_9, \varphi' = Y_{10}, \varphi'' = Y_{10}', \quad (20)$$

$$\xi = Y_{11}, \xi' = Y_{12}, \xi'' = Y_{12}'.$$

Using the above expressions in MATLAB `bvp4c` we have the following set of first-order equations:

$$Y_3' = [(1-n)/nWeY_3[(Y_4 + Y_1)Y_3 + \lambda * Y_2 + F_r Y_2^2 + Y_2^2 + Y_5 Y_2 - \frac{M^2}{\beta_e^2 + (1 + \beta_e \beta_i)^2} (Y_5 \beta_e - Y_2(1 + \beta_i \beta_e))], \quad (21)$$

$$Y_6' = [(1-n)/nWeY_6][(Y_4 + Y_1)Y_6 + \lambda * Y_5 + F_r Y_5^2 + Y_5^2 + Y_5 Y_2 + \frac{M^2}{\beta_e^2 + (1 + \beta_e \beta_i)^2} (Y_2 \beta_e + Y_5(1 + \beta_i \beta_e))], \quad (22)$$

$$Y_8' = [(Y_4 + Y_1)(Y_2 + Y_5)Y_8 - QY_7 + Y_2^2 + Y_5 Y_2 - \frac{M^2}{\beta_e^2 + (1 + \beta_e \beta_i)^2} (Y_5 \beta_e - Y_2(1 + \beta_i \beta_e)) - N_b Y_8 Y_{10} - N_t Y_8^2 - \frac{M^2 Ec}{\beta_e^2 + (1 + \beta_e \beta_i)^2} (Y_5^2 + Y_2^2) - (Y_1 + Y_4)Y_8] / \left[\frac{1}{Pr} - \lambda_1(Y_4 + Y_1) \right], \quad (23)$$

$$Y_{10}' = -Sc(Y_1 + Y_4)Y_{10} - \frac{N_t}{N_b} Y_8' + K_r Sc Y_9 (1 + \delta Y_7)^n e^{\frac{-E}{1+\delta Y_7}}, \quad (24)$$

$$Y_{12}' = -Lb(Y_4 + Y_1)\xi' + Pe[(\Omega + \xi)Y_{10}' + \xi'Y_9], \quad (25)$$

with the transformed BCs

$$Y_1(0) = Y_2(\infty) = 0, Y_2(0) = 1, Y_4(0) = Y_5(\infty) = 0, Y_5(0) = \lambda, Y_7(0) = -Bi(1 - Y_8(0)), \quad (26)$$

$$Y_9(0) = 1 + BY_{10}(0), Y_{11}(0) = 1; Y_7(\infty) = 0, Y_9(\infty) = 0, Y_{11}(\infty) = 0.$$

Results and discussion

This segment (Figs. 2, 3, 4, 5, 6, 7, 8, 9, 10, 11, 12, 13, 14) is designed to discuss the salient features of the prominent arising parameters versus the allied profiles. The admissible ranges of the parameters are taken where the resolution of the graphs is best suited. These are $0.0 \leq M \leq 1.6, 0.0 \leq We \leq 1.5, 0.0 \leq \beta_e \leq 1.2,$

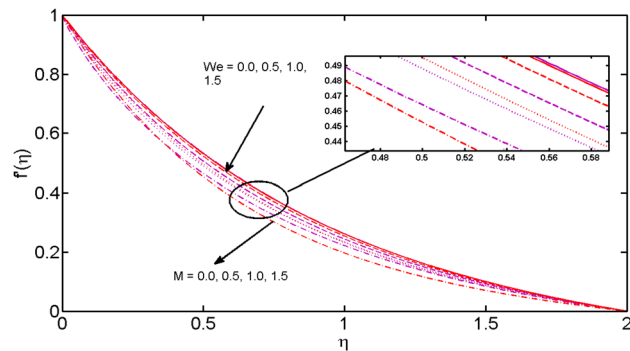


Figure 2. M and We variations vs. $f'(\eta)$.

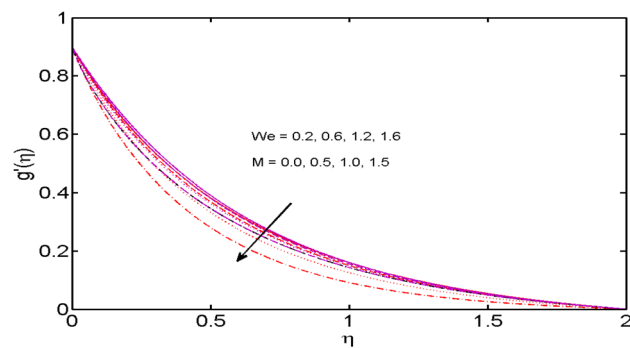


Figure 3. M and We variations vs. $g'(\eta)$.

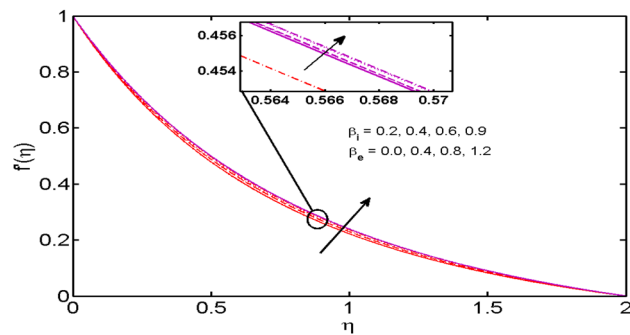


Figure 4. β_i and β_e variations vs. $f'(\eta)$.

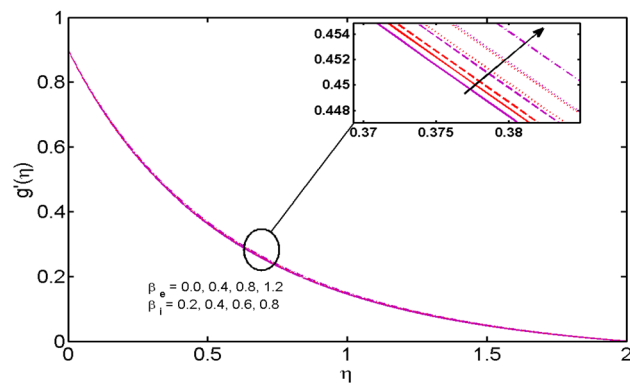


Figure 5. β_i and β_e variations vs. $g'(\eta)$.

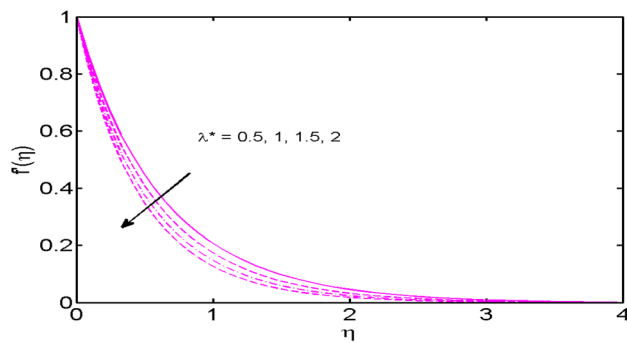


Figure 6. λ^* variations vs. $f'(\eta)$.

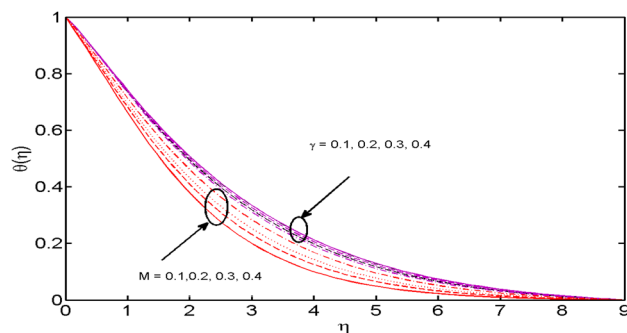


Figure 7. M and γ variations vs. $\theta(\eta)$.

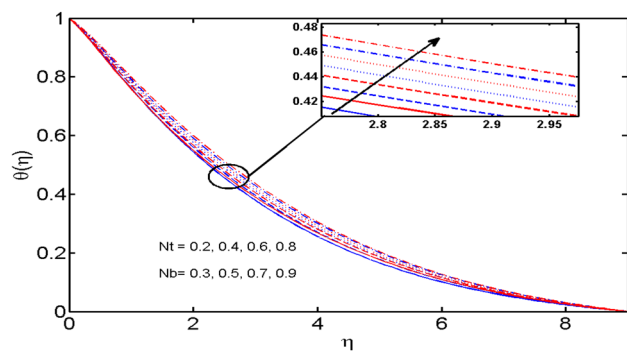


Figure 8. N_t and N_b variations vs. $\theta(\eta)$.

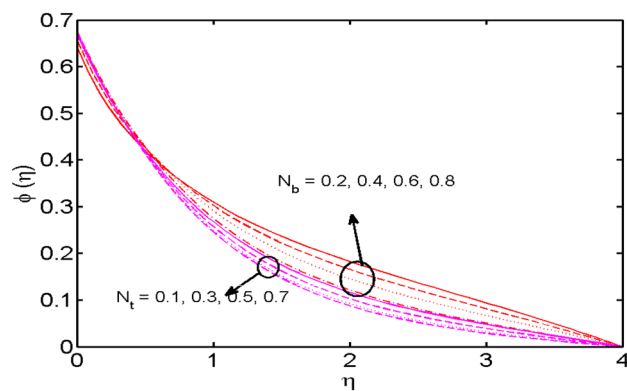


Figure 9. N_t and N_b variations vs. $\phi(\eta)$.

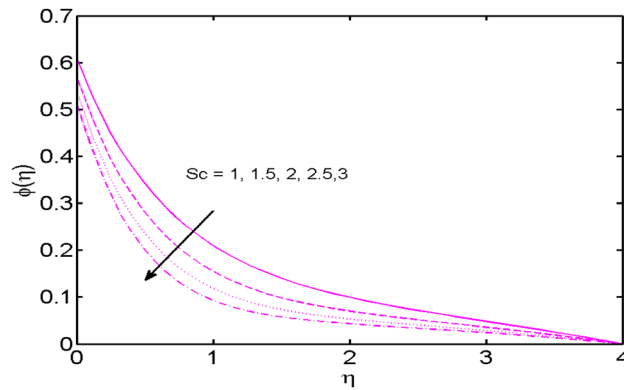


Figure 10. Sc variations vs. $\varphi(\eta)$.

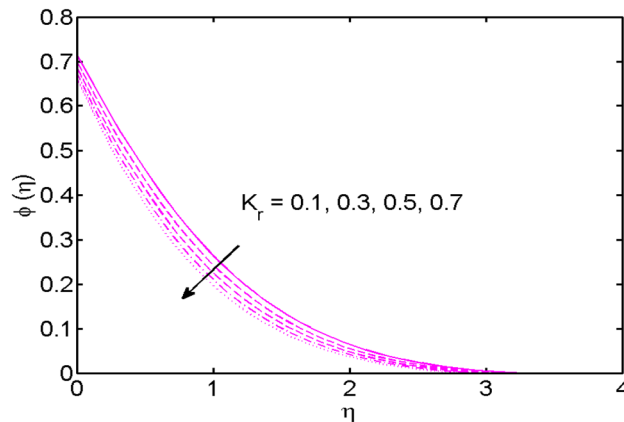


Figure 11. K_r variations vs. $\varphi(\eta)$.

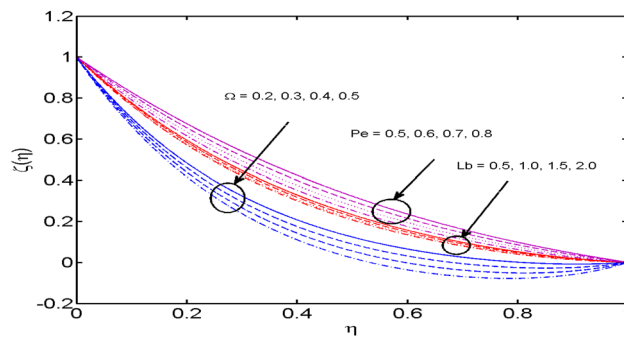


Figure 12. Ω, P_e and L_b variations vs. $\xi(\eta)$.

$0.2 \leq \beta_i \leq 0.9, 0.5 \leq \lambda^* \leq 2.0, 0.1 \leq \gamma \leq 0.4, 0.1 \leq N_t \leq 0.8, 0.2 \leq N_b \leq 0.9, 1.0 \leq S_c \leq 3.0, 0.1 \leq K_r \leq 0.7, 0.2 \leq \Omega \leq 0.5, 0.5 \leq P_e \leq 0.8, 0.5 \leq L_b \leq 2.0, 0.3 \leq E \leq 1.2, 0.1 \leq B_i \leq 0.9$. Figures 2 and 3 are illustrated to witness the behavior of the magnetic parameter M and Weissenberg number We on the velocity profiles in both directions. It is noticed that the velocity profiles $f'(\eta)$ and $g'(\eta)$ are decreased for large estimates of M and We . The fluid velocity in both directions is reduced owing to strong Lorentz force that hinders the movement of the fluid. The Weissenberg number is the quotient of elastic to the viscous forces⁴⁸. Large estimates of We mean the significant upturn in the elastic forces. Thus, increasing the relaxation time and eventually, decreased velocity in both directions is witnessed.

The effects of the Hall parameter $\beta_e (= \omega_e \tau_e)$, and slip parameter $\beta_i (= \omega_i \tau_i)$, on the velocity profiles in both x - and y -directions are depicted in Figs. 4 and 5 respectively. As the Hall parameter $\beta_e (= \omega_e \tau_e)$, is defined as

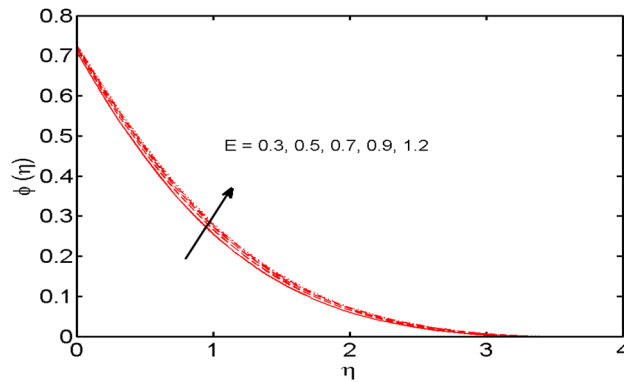


Figure 13. E variations vs. $\phi(\eta)$.

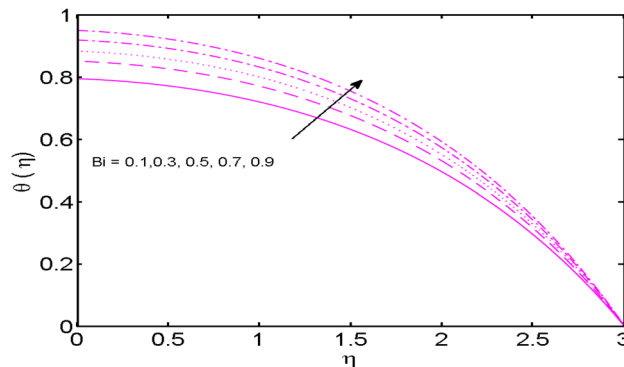


Figure 14. Bi variations vs. $\theta(\eta)$.

the product of electrons' frequency and electrons' collisions time. An upsurge in β_e means either of electrons' frequency or electron collisions time is escalated or values of both are augmented. It is also verified truth that magnetic and the Hall forces are opposite to each other. As discussed above that magnetic forces oppose the fluid motion. Thus, following the definition, the Hall effect assists the fluid velocity. Similar behavior is comprehended for slip parameter $\beta_i (= \omega_i \tau_i)$, in x - and y -directions (Fig. 5). Figure 6 reveals that the variation of the velocity profile for changed estimation of the porosity parameter. It is witnessed that for higher values of the porosity parameter, the velocity profile declines.

In Fig. 7, temperature behavior for varied estimates of the magnetic parameter M and thermal relaxation parameter γ is depicted. From the figure, it is seen that the temperature profile is a declining function of respective relaxation time. Higher estimates of relaxation time result in the insulating behavior of the material which is accountable for a decrease in fluid temperature. However, the opposite trend is perceived in the case of a magnetic parameter. Here, for growing values of M , the temperature of the fluid is on rising owing to a thickening effect on the thermal boundary layer which is the result of a strong magnetic field.

The effects of the Brownian motion parameter N_b and the Thermophoresis parameter N_t on the temperature profile are depicted in Fig. 8. The higher temperature is noticed for greater estimation of both N_b and N_t . This is because the random motion of fluid particles generates more heat and as a result temperature distribution is increased. Similarly, it is observed that the growing estimation of N_t boost up the temperature profile. This is because of enhancement in N_t push the nanoparticles of fluid away from the hot surface which causes enhancement in temperature profiles.

The impact of the same parameters *i.e.*, Brownian motion parameter N_b and the Thermophoresis parameter N_t on the concentration distribution are displayed in Fig. 9. It is comprehended that the Brownian motion parameter and the Thermophoresis parameter have escalating and diminishing effects on the concentration profile respectively. Large Brownian motion means the more random motion of fluid particles thus strengthening the concentration of the fluid and an opposing impact is visualized for the thermophoretic parameter on the fluid's concentration. All these findings are according to the recently published articles^{12,49,50}.

Figure 10 is outlined to learn the influence of Schmidt number Sc against the concentration field. For higher estimates of Sc anemic concentration is noted. Schmidt number is in inverse proportionate to Brownian diffusivity. Mounting estimates of Sc results in lowering the Brownian diffusivity. Eventually, this feeble Brownian diffusivity diminishes the concentration profile.

The impact of the chemical reaction parameter K_r on the concentration field is witnessed in Fig. 11. It is noted that nanoparticles volume concentration diminishes for large estimates of $K_r > 0$, *i.e.*, destructive case.

M	Ec	Pr	We	β_e	β_i	$-\sqrt{Re}C_{fx}$	$-\sqrt{Re}C_{gy}$
0	3	3	1	1.2	0.9	1.3748921	0.70471084
0.5						1.3891760	0.72841397
0.7						1.4028943	0.75088802
0.9						1.4211882	0.78043358
0.5	1					1.3891760	0.72841397
	2					1.3891760	0.72841397
	3					1.3891760	0.72841397
	4					1.3891760	0.72841397
	3	1				1.3891764	0.72841397
		2				1.3891764	0.72841397
		3				1.3891764	0.72841397
		4				1.3891764	0.72841397
		3	1			1.389176	0.72841397
			2			1.3117802	0.70827679
			3			1.2240033	0.68654032
			4			0.78790504	0.67413247
			1	0.6		1.4005879	0.73505713
				1		1.3918829	0.73046773
				1.5		1.3862657	0.72576016
				2.1		1.3827605	0.72175107
				1.2	0.2	1.3861825	0.74221885
					0.5	1.3885132	0.73530222
					0.7	1.3890701	0.73155041
					0.9	1.3891760	0.72841397

Table 1. Numerical values of Drag force $C_f Re_x^{1/2}$ against the varied values of the rising parameter.

For growing values of $K_r > 0$, the chemical reaction in case of the destructive case creates much disturbance as compared to the generative case. Therefore, the molecular movement $K_r > 0$ is much larger and creates an escalation in mass transport. Eventually, nanoparticles volume concentration decreases.

The variation of Peclet number Pe , Bio convection Lewis number Lb , and the Microorganisms concentration difference parameter Ω on motile density profile is demonstrated in Fig. 12. It is noted that the motile density profile decreases for large estimates of the Bio-convection Peclet number. A rise in Pe results in a decline in the diffusivity of microorganisms and thus the motile density of liquid falls. Figure 10 also highlights the influence of Microorganisms concentration difference parameter and bio-convection Lewis number on motile density profile. It is observed that the rise in Ω improves the concentration of microorganisms in the ambient boundary layer and reduces the density profile. Also, for growing values of Lb , the diffusivity of microorganisms declines and therefore the motile density decays.

The role of the activation energy parameter E versus the concentration profile is portrayed in Fig. 13. It is comprehended that the concentration is strengthened when estimates of E are enhanced. The generative chemical reaction is boosted when values of E are enhanced. Thus, improvement in concentration is monitored.

The conduct of the Biot number Bi on temperature distribution is examined in Fig. 14. It is seen that, temperature and thickness of the thermal boundary layer upsurge for higher estimates of Bi . Here, the expansion in Bi instigates the heat transfer coefficient which pushes more heat from the surface to the fluid. This outcome is consistent with the published result³⁸. In this way, the temperature is enhanced. It is also noticed that $Bi = 0$ is associated with an insulated wall while $Bi \rightarrow \infty$ act as the constant wall temperature. Higher estimations of Bi turn out as a higher rate of heat transfer. So, Bi can be adopted as a cooling operator in the advanced procedures.

Tables 1 and 2 represent the numerical outcomes of the surface drag force coefficients in both directions and rate of mass flux for different estimates of emerging parameters Hall parameter β_e , ion slip parameter β_i , magnetic parameter M , Prandtl number Pr , Eckert number Ec , and Weissenberg number We . It is witnessed that surface drag force coefficient in x -direction decrease when Hall parameter, Weissenberg number, are increased and an opposite tendency is noted for the magnetic parameter, and ion slip parameter. The surface drag force coefficient in y -direction is increased for mounting estimates of the magnetic parameter, and an opposing tendency is perceived for growing values of slip and the Hall parameters. However, Table 2 depicts the variations in the rate of mass flux for varied values of E , K , and N_t . It is comprehended that for the higher estimates of K and N_t , rate of mass flux escalate and an opposing impact is seen for the values of E . Table 3 reveals the behavior of several parameters on the local density number of motile microorganisms. It is examined that for higher estimates of Pe and Ω , the local density number of motile microorganisms' upsurges while decreases for higher Lb number.

The presented model is compared with Wang⁵¹ (Table 4) in limiting the case. An excellent correlation between the two results is found. The particularly, partially ionized assumption is set to zero. Moreover, the assumption of Bioconvection is also reduced to zero. Thus, making the referred problem similar to the given model here, all

E	K	N_t	$Sh_x Re^{-0.5}$
0.4	0.3	0.01	1.396003486334218
0.5			1.382339484071596
0.6			1.369614279513656
0.4	0.4		1.453495332636076
	0.5		1.547835760678850
	0.6		1.720996325877767
	0.3	0.02	1.398055545440856
		0.03	1.400127349140989
		0.04	1.402218982444583

Table 2. Numerical values for $Sh_x Re^{-0.5}$ against the different estimations of the rising parameter.

Lb	Pe	Ω	$Nn_x Re_x^{-1/2}$
0.4	0.3	0.2	1.337005640792250
0.5			1.329845324236785
0.6			1.322647053220159
0.4	0.4		1.426874259673157
	0.5		1.519142631773676
	0.6		1.613768570127874
	0.3	0.2	1.337005640792250
		0.3	1.344975671529449
		0.4	1.352945702320629

Table 3. Numerical values for $Nn_x Re_x^{-1/2}$ against the different values of the rising parameter.

λ	⁵¹	Present	⁵¹	Present	⁵¹	Present	⁵¹	Present
	$f''(0)$	$f''(0)$	$g''(0)$	$g''(0)$	$f(\infty)$	$f(\infty)$	$g(\infty)$	$g(\infty)$
0	-1	-1	0	0	1	1	0	0
0.25	-1.048813	-1.048793	-0.194564	-0.194543	0.907075	0.907053	0.257986	0.257981
0.50	-1.093097	-1.093081	-0.465205	-0.465187	0.842360	0.842323	0.451671	0.451623
0.75	-1.134485	-1.134456	-0.794622	-0.794602	0.792308	0.792293	0.612049	0.612021
1.00	-1.173720	-1.173698	-1.173720	-1.173711	0.751527	0.751502	0.751527	0.751511

Table 4. Comparison between values of $f''(0)$, $g''(0)$, $f(\infty)$, and $g(\infty)$ with Wang⁵¹ for numerical values for λ .

extra assumptions are discarded. On comparing the values of $f''(0)$, $g''(0)$, $f(\infty)$, and $g(\infty)$ for varied values of stretching ratio parameter λ . An outstanding correlation between the two results is accomplished.

Final remarks

In this article, steady 3D Tangent hyperbolic nanofluid flow with Hall and Ion slip over a linear bi-directional stretchable surface with Cattaneo–Christov heat flux in a Darcy–Forchheimer permeable medium had been analyzed. Additional effects of heat generation/absorption, bioconvective gyrotactic microorganisms, and chemical reaction with activation energy are also considered. The partially ionized Tangent hyperbolic nanofluid flow amalgamated with chemical reaction with activation energy. The slip and convective conditions are taken at the boundary. The numerical solution of the problem is achieved by using the bvp4c MATLAB technique. The fluid model is unique in its way and has not been discussed in the literature yet. The significant observations (answer to the aforementioned questions) of the model are appended as follows:

- The velocity of the liquid is increased for sizeable values of the ion slip parameter.
- The concentration is strengthened when the values of the activation energy parameter are enhanced.
- The motile density profile is a diminishing function of Peclet and Bioconvection Lewis numbers. Bioconvection microorganisms possess numerous applications in varied engineering disciplines including soil, genetic, wastewater, and microbial, etc.
- The temperature of the liquid augments for the strong magnetic field.

- The velocity profiles are the diminishing function of the magnetic parameter.
- The temperature is decreased for high thermal relaxation parameter values.
- The temperature profile shows dominance for large estimates of Brownian motion and thermophoresis parameters.

Future possibilities

The envisaged mathematical model may be extended in the following ways:

- The effects of homogeneous–heterogeneous reactions may be considered by replacing the bio-convective relation.
- Some other non-Newtonian fluid may also be considered for the Tangent hyperbolic fluid.
- The Buongiorno model may be replaced by Tiwari and Das model.
- In Tiwari and Das model numerous combinations of nanoparticles and base fluids may be considered.
- The geometry of the problem may also be changed.

Received: 18 June 2020; Accepted: 11 September 2020

Published online: 27 October 2020

References

1. Shafiq, A., Hammouch, Z. & Sindhu, T. N. Bioconvective MHD flow of tangent hyperbolic nanofluid with Newtonian heating. *Int. J. Mech. Sci.* **133**, 759–766 (2017).
2. Hayat, T., Waqas, M., Alsaedi, A., Bashir, G. & Alzahrani, F. Magnetohydrodynamic (MHD) stretched flow of tangent hyperbolic nano liquid with variable thickness. *J. Mol. Liq.* **229**, 178–184 (2017).
3. Ibrahim, W. & Gizewu, T. Tangent hyperbolic nanofluid with mixed convection flow: An application of improved Fourier and Fick's diffusion model. *Heat Transf. Asian Res.* **48**(8), 4217–4239 (2019).
4. Ramzan, M., Gul, H. & Sheikholeslami, M. Effect of second-order slip condition on the flow of tangent hyperbolic fluid—A novel perception of Cattaneo–Christov heat flux. *Phys. Scr.* **94**(11), 115707 (2019).
5. Maqbool, K., Shaheen, S. & Siddiqui, A. M. Effect of nano-particles on MHD flow of tangent hyperbolic fluid in a ciliated tube: An application to fallopian tube. *Math. Biosci. Eng. MBE.* **16**(4), 2927–2941 (2019).
6. Zaib, A., Khan, U., Wakif, A., & Zaydan, M. Numerical entropic analysis of mixed MHD convective flows from a non-isothermal vertical flat plate for radiative tangent hyperbolic blood biofluids conveying magnetite ferroparticles: Dual similarity solutions. *Arab. J. Sci. Eng.* **45**, 1–20 (2020).
7. Jabeen, S., Hayat, T., Qayyum, S. & Alsaedi, A. Significance of activation energy in stratified flow of tangent hyperbolic fluid. *Int. J. Numer. Methods Heat Fluid Flow* **29**, 2932–2947 (2019).
8. Nayak, M. K., Shaw, S., Makinde, O. D. & Chamkha, A. J. Investigation of partial slip and viscous dissipation effects on the radiative tangent hyperbolic nanofluid flow past a vertical permeable Riga plate with internal heating: Buongiorno model. *J. Nanofluids.* **8**(1), 51–62 (2019).
9. Al-Khaled, K., Khan, S. U. & Khan, I. Chemically reactive bioconvection flow of tangent hyperbolic nanofluid with gyrotactic microorganisms and nonlinear thermal radiation. *Heliyon.* **6**(1), e03117 (2020).
10. Awad, F. G., Motsa, S. & Khumalo, M. Heat and mass transfer in unsteady rotating fluid flow with binary chemical reaction and activation energy. *PLoS ONE* **9**(9), e107622 (2014).
11. Lu, D., Ramzan, M., Ullah, N., Chung, J. D. & Farooq, U. A numerical treatment of radiative nanofluid 3D flow containing gyrotactic microorganism with anisotropic slip, binary chemical reaction and activation energy. *Sci. Rep.* **7**(1), 1–22 (2017).
12. Khan, N. S., Kumam, P. & Thounthong, P. Second law analysis with effects of Arrhenius activation energy and binary chemical reaction on nanofluid flow. *Sci. Rep.* **10**(1), 1–16 (2020).
13. Koriko, O. K., Omowaye, A. J., Animasaun, I. L. & Babatunde, I. O. Boundary layer analysis of exothermic and endothermic kind of chemical reaction in the flow of non-Darcian unsteady micropolar fluid along an infinite vertical surface. *Int. J. Eng. Res. Afr.* **28**, 90–101 (2017).
14. Ramzan, M., Ullah, N., Chung, J. D., Lu, D. & Farooq, U. Buoyancy effects on the radiative magneto Micropolar nanofluid flow with double stratification, activation energy and binary chemical reaction. *Sci. Rep.* **7**(1), 1–15 (2017).
15. Shah, Z., Kumam, P. & Deebani, W. Radiative MHD Casson nanofluid flow with activation energy and chemical reaction over past nonlinearly stretching surface through Entropy generation. *Sci. Rep.* **10**(1), 1–14 (2020).
16. Azam, M., Xu, T., Shakoor, A. & Khan, M. Effects of Arrhenius activation energy in development of covalent bonding in axisymmetric flow of radiative-Cross nanofluid. *Int. Commun. Heat Mass Transf.* **113**, 104547 (2020).
17. Kuznetsov, A. V. The onset of nanofluid bioconvection in a suspension containing both nanoparticles and gyrotactic microorganisms. *Int. Commun. Heat Mass Transf.* **37**(10), 1421–1425 (2010).
18. Kuznetsov, A. V. Nanofluid bioconvection in water-based suspensions containing nanoparticles and oxytactic microorganisms: Oscillatory instability. *Nanoscale Res. Lett.* **6**(1), 100 (2011).
19. Kuznetsov, A. V. Non-oscillatory and oscillatory nanofluid bio-thermal convection in a horizontal layer of finite depth. *Eur. J. Mech. B Fluids.* **30**(2), 156–165 (2011).
20. Aziz, A., Khan, W. A. & Pop, I. Free convection boundary layer flow past a horizontal flat plate embedded in porous medium filled by nanofluid containing gyrotactic microorganisms. *Int. J. Therm. Sci.* **56**, 48–57 (2012).
21. Akbar, N. S. & Khan, Z. H. Magnetic field analysis in a suspension of gyrotactic microorganisms and nanoparticles over a stretching surface. *J. Magn. Magn. Mater.* **410**, 72–80 (2016).
22. Alsaedi, A., Khan, M. I., Farooq, M., Gull, N. & Hayat, T. Magnetohydrodynamic (MHD) stratified bioconvective flow of nanofluid due to gyrotactic microorganisms. *Adv. Powder Technol.* **28**(1), 288–298 (2017).
23. Khan, M., Irfan, M. & Khan, W. A. Impact of nonlinear thermal radiation and gyrotactic microorganisms on the Magneto-Burgers nanofluid. *Int. J. Mech. Sci.* **130**, 375–382 (2017).
24. Begum, N., Siddiqua, S. & Hossain, M. A. Nanofluid bioconvection with variable thermophysical properties. *J. Mol. Liq.* **231**, 325–332 (2017).
25. Kumar, P. S., Gireesha, B. J., Mahanthesh, B. & Chamkha, A. J. Thermal analysis of nanofluid flow containing gyrotactic microorganisms in bioconvection and second-order slip with convective condition. *J. Therm. Anal. Calorim.* **136**(5), 1947–1957 (2019).
26. Ramzan, M., Chung, J. D. & Ullah, N. Radiative magnetohydrodynamic nanofluid flow due to gyrotactic microorganisms with chemical reaction and non-linear thermal radiation. *Int. J. Mech. Sci.* **130**, 31–40 (2017).

27. Bhatti, M. M., Riaz, A., Zhang, L., Sait, S. M., & Ellahi, R. Biologically inspired thermal transport on the rheology of Williamson hydromagnetic nanofluid flow with convection: An entropy analysis. *J. Therm. Anal. Calorim.* <https://doi.org/10.1007/s10973-020-09876-5> (2020).
28. Zhang, L., Arain, M. B., Bhatti, M. M., Zeeshan, A. & Hal-Sulami, H. Effects of magnetic Reynolds number on swimming of gyrotactic microorganisms between rotating circular plates filled with nanofluids. *Appl. Math. Mech.* **41**(4), 637–654 (2020).
29. Makinde, O. D. & Animasaun, I. L. Bioconvection in MHD nanofluid flow with nonlinear thermal radiation and quartic autocatalysis chemical reaction past an upper surface of a paraboloid of revolution. *Int. J. Therm. Sci.* **109**, 159–171 (2016).
30. Cramer, K. R. & Pai, S. I. *Magnetofluid Dynamics for Engineers and Applied Physicists* (Scripta Publishing Company, Texas, 1973).
31. Abdelsalam, S. I. & Bhatti, M. M. The study of non-Newtonian nanofluid with hall and ion slip effects on peristaltically induced motion in a non-uniform channel. *RSC Adv.* **8**(15), 7904–7915 (2018).
32. Nawaz, M., Rana, S., Qureshi, I. H. & Hayat, T. Three-dimensional heat transfer in the mixture of nanoparticles and micropolar MHD plasma with Hall and ion slip effects. *AIP Adv.* **8**(10), 105109 (2018).
33. Animasaun, I. L. *et al.* Comparative analysis between 36 nm and 47 nm alumina–water nanofluid flows in the presence of Hall effect. *J. Therm. Anal. Calorim.* **135**(2), 873–886 (2019).
34. Mahanthesh, B., Shashikumar, N. S., Gireesha, B. J. & Animasaun, I. L. Effectiveness of Hall current and exponential heat source on unsteady heat transport of dusty TiO₂-EO nanoliquid with nonlinear radiative heat. *J. Comput. Des. Eng.* **6**(4), 551–561 (2019).
35. Bhatti, M. M., Ellahi, R., Zeeshan, A., Marin, M. & Ijaz, N. Numerical study of heat transfer and Hall current impact on peristaltic propulsion of particle-fluid suspension with compliant wall properties. *Mod. Phys. Lett. B* **33**(35), 1950439 (2019).
36. Wakif, A., Chamkha, A., Thumma, T., Animasaun, I. L., & Sehaqui, R. Thermal radiation and surface roughness effects on the thermo-magneto-hydrodynamic stability of alumina–copper oxide hybrid nanofluids utilizing the generalized Buongiorno’s nanofluid model. *J. Therm. Anal. Calorim.* <https://doi.org/10.1007/s10973-020-09488-z> (2020).
37. Wakif, A., Boulahia, Z., Mishra, S. R., Rashidi, M. M. & Sehaqui, R. Influence of a uniform transverse magnetic field on the thermo-hydrodynamic stability in water-based nanofluids with metallic nanoparticles using the generalized Buongiorno’s mathematical model. *Eur. Phys. J. Plus.* **133**(5), 181 (2018).
38. Rasool, G., & Wakif, A. Numerical spectral examination of EMHD mixed convective flow of second-grade nanofluid towards a vertical Riga plate using an advanced version of the revised Buongiorno’s nanofluid model. *J. Therm. Anal. Calorim.* <https://doi.org/10.1007/s10973-020-09865-8> (2020).
39. Nayak, M. K., Wakif, A., Animasaun, I. L., & Alaoui, M. S. H. Numerical differential quadrature examination of steady mixed convection nanofluid flows over an isothermal thin needle conveying metallic and metallic oxide nanomaterials: a comparative investigation. *Arab. J. Sci. Eng.* **45**, 5331–5346 (2020).
40. Shafee, A., Allahyari, M., Ramzan, M., Zaib, A., & Babazadeh, H. Modeling of MHD hybrid nanofluid flow through permeable enclosure. *Int. J. Mod. Phys. C* **31**(8), 2050106 (2020).
41. Ramzan, M., Riasat, S., Shah, Z., Kumam, P., & Thounthong, P. Unsteady MHD carbon nanotubes suspended nanofluid flow with thermal stratification and nonlinear thermal radiation. *Alex. Eng. J.* **59**(3), 1557–1566 (2020).
42. Babazadeh, H., Muhammad, T., Shakeriaski, F., Ramzan, M., & Hajizadeh, M. R. Nanomaterial between two plates which are squeezed with impose magnetic force. *J. Therm. Anal. Calorim.* <https://doi.org/10.1007/s10973-020-09619-6> (2020).
43. Tlili, I. *et al.* A novel model to analyze Darcy Forchheimer nanofluid flow in a permeable medium with Entropy generation analysis. *J. Taibah Univ. Sci.* **14**(1), 916–930 (2020).
44. Tlili, I., Ramzan, M., Kadry, S., Kim, H. W. & Nam, Y. Radiative MHD nanofluid flow over a moving thin needle with Entropy generation in a porous medium with dust particles and Hall current. *Entropy.* **22**(3), 354 (2020).
45. Suleman, M. *et al.* Entropy analysis of 3D non-Newtonian MHD nanofluid flow with nonlinear thermal radiation past over exponential stretched surface. *Entropy.* **20**(12), 930 (2018).
46. Ramzan, M. *et al.* Impact of nonlinear chemical reaction and melting heat transfer on an MHD nanofluid flow over a thin needle in porous media. *Appl. Sci.* **9**(24), 5492 (2019).
47. Nawaz, M., Qureshi, I. H. & Shahzad, A. Thermal performance of partially ionized Eyring–Powell liquid: a theoretical approach. *Phys. Scr.* **94**(12), 125209 (2019).
48. Poole, R. J. The Deborah and Weissenberg numbers. *Rheol. Bull.* **53**(2), 32–39 (2012).
49. Wakif, A., Animasaun, I. L., & Sarojamma, G. Meta-analysis on thermo-migration of tiny/nano-sized particles in the motion of various fluids. *Chin. J. Phys.* <https://doi.org/10.1016/j.cjph.2019.12.002> (2019).
50. Animasaun, I. L., Ibraheem, R. O., Mahanthesh, B. & Babatunde, H. A. A meta-analysis on the effects of haphazard motion of tiny/nano-sized particles on the dynamics and other physical properties of some fluids. *Chin. J. Phys.* **60**, 676–687 (2019).
51. Wang, C. Y. The three dimensional flow due to a stretching flat surface. *Phys. Fluids.* **27**(8), 1915–1917 (1984).

Acknowledgements

This research was supported by Basic Science Research Program through the National Research Foundation of Korea (NRF) funded by the Ministry of Education (No. 2017R1D1A1A1B05030422).

Author contributions

Conceptualization, M.R.; methodology, H.G.; validation, S.K.; formal analysis, Y.M.C.; writing—original draft preparation, H.G.; writing—review and editing, M.R.; supervision; revised manuscript editing, J.D.C.; funding acquisition, J.D.C.

Competing interests

The authors declare no competing interests.

Additional information

Correspondence and requests for materials should be addressed to Y.-M.C.

Reprints and permissions information is available at www.nature.com/reprints.

Publisher’s note Springer Nature remains neutral with regard to jurisdictional claims in published maps and institutional affiliations.



Open Access This article is licensed under a Creative Commons Attribution 4.0 International License, which permits use, sharing, adaptation, distribution and reproduction in any medium or format, as long as you give appropriate credit to the original author(s) and the source, provide a link to the Creative Commons licence, and indicate if changes were made. The images or other third party material in this article are included in the article's Creative Commons licence, unless indicated otherwise in a credit line to the material. If material is not included in the article's Creative Commons licence and your intended use is not permitted by statutory regulation or exceeds the permitted use, you will need to obtain permission directly from the copyright holder. To view a copy of this licence, visit <http://creativecommons.org/licenses/by/4.0/>.

© The Author(s) 2020